Front. Chem. Sci. Eng. 2018, 12(1): 83–93
https://doi.org/10.1007/s11705-017-1691-6

RESEARCH ARTICLE

Al_2O_3 and CeO_2-promoted MgO sorbents for CO_2 capture at moderate temperatures

Huimei Yu[1,2,3], Xiaoxing Wang (✉)[1], Zhu Shu[2], Mamoru Fujii[1], Chunshan Song (✉)[1]

1 EMS Energy Institute, PSU-DUT Joint Center for Energy Research, and Department of Energy & Mineral Engineering, Pennsylvania State University, University Park 16802, USA
2 Shanghai Institute of Ceramics, Chinese Academy of Sciences, Shanghai 200050, China
3 East China University of Science and Technology, Shanghai 200237, China

© Higher Education Press and Springer-Verlag GmbH Germany, part of Springer Nature 2018

Abstract A series of Al_2O_3 and CeO_2 modified MgO sorbents was prepared and studied for CO_2 sorption at moderate temperatures. The CO_2 sorption capacity of MgO was enhanced with the addition of either Al_2O_3 or CeO_2. Over Al_2O_3-MgO sorbents, the best capacity of 24.6 mg-CO_2/g-sorbent was attained at 100 °C, which was 61% higher than that of MgO (15.3 mg-CO_2/g-sorbent). The highest capacity of 35.3 mg-CO_2/g-sorbent was obtained over the CeO_2-MgO sorbents at the optimal temperature of 200 °C. Combining with the characterization results, we conclude that the promotion effect on CO_2 sorption with the addition of Al_2O_3 and CeO_2 can be attributed to the increased surface area with reduced MgO crystallite size. Moreover, the addition of CeO_2 increased the basicity of MgO phase, resulting in more increase in the CO_2 capacity than Al_2O_3 promoter. Both the Al_2O_3-MgO and CeO_2-MgO sorbents exhibited better cyclic stability than MgO over the course of fifteen CO_2 sorption-desorption cycles. Compared to Al_2O_3, CeO_2 is more effective for promoting the CO_2 capacity of MgO. To enhance the CO_2 capacity of MgO sorbent, increasing the basicity is more effective than the increase in the surface area.

Keywords CO_2 capture, MgO sorbents, Al_2O_3, CeO_2, flue gas

1 Introduction

Global climate change due to increasing anthropogenic CO_2 emissions has aroused worldwide concern. Carbon capture and storage (CCS) is considered a promising option for mitigating CO_2 emissions [1–3]. Thus CCS has become an important area of research [3], especially CO_2 captured from large emission sources such as fossil fuel power plants. With this goal in mind, many CO_2 separation approaches have been investigated and these can be divided into three major types: post-combustion decarbonization, pre-combustion decarbonization and oxy-fuel combustion. The methods developed for CO_2 removal from post-combustion flue gases and/or pre-combustion syngas streams include absorption with liquid solvents [4,5], membrane separations [6,7], cryogenic distillations [7,8], and adsorption with carbon materials and molecular sieves [9–11]. However, these methods are either costly due to significant energy consumption or limited by the fairly high temperatures of the flue gases.

To improve the energy efficiency and reduce cost, many solid sorbents have been reported and these can be classified into four categories which are based on their operating temperatures: low (below room temperature), ambient (between room temperature and 100 °C), moderate (between 100 and 400 °C) and high (above 400 °C). Zeolites [4,12], metal-organic frameworks (MOFs) [13,14] and carbon materials [15] are the typical adsorbents for the low temperature category, which is based on physisorption. Although a very high CO_2 capacity of 1320 mg-CO_2/g-S (S = sorbent) has been reported for MOF-5 (at –53 °C) [16], the large reduction of CO_2 capacity at elevated temperatures and the negative impact of moisture greatly limits the application of these materials to CO_2 capture from flue gases. In the ambient-temperature category, amine-based solid sorbents [2,3,17–20] have received significant attention and are promising alternatives for CO_2 capture due to their high capacities ($>$ 100 mg-CO_2/g-S), high selectivities and good regenerabilities. Moisture even showed positive effect over these sorbents [21]. In the high-temperature-adsorbent category, Li- [22] and Ca-based [23,24] adsorbents have high CO_2 capacities although temperatures above 800 °C are

Received July 27, 2017; accepted October 11, 2017

E-mails: xxwang@psu.edu (Wang X), csong@psu.edu (Song C)

normally required for their regeneration. Since the temperature of the flue gas vent is usually in the range of 150–400 °C [25], the use of moderate temperature sorbents would seem to be the most suitable. Consequently, sorbents containing alkali or alkaline-earth metals such as Na_2CO_3, K_2CO_3, and MgO have attracted increasing attention since they can be operated at moderate temperatures (100–400 °C) and are applicable to both post- and pre-combustion capture [26,27].

Among the alkaline-earth metal oxides, magnesium oxide is a good candidate for CO_2 capture because of its low cost, abundance, and low toxicity [27]. Compared to CaO-based sorbents, MgO can capture CO_2 at temperatures lower than 200 °C and be regenerated at low temperatures (e.g., 300–500 °C). This is beneficial because a lower temperature not only greatly reduces energy costs but also reduces sintering issues caused by high operating temperatures. In addition, MgO has a high potential for CO_2 sorption. On the basis of the reversible chemical reaction between CO_2 and magnesium oxide:

$$MgO + CO_2 \leftrightarrow MgCO_3 (H^{o}_{298\,K} = -100.8\,kJ/mol) \quad (1)$$

the theoretical CO_2 capture capacity of MgO could be as high as 1100 mg-CO_2/g-S. However, several research groups have reported that MgO alone has a very low sorption capacity (5.7, 8.8 and 3.6 mg-CO_2/g-S) [28]. There are two ways to improve the sorption capacity of MgO sorbents. One is to increase the surface area which allows for more efficient interfacial contacts between the MgO and CO_2. This can be accomplished by either dispersing MgO on a high surface area support or by preparing mesoporous MgO materials like carbon supported MgO sorbents [28,29], mesoporous silica supported MgO sorbents [30], MgO/Al_2O_3 sorbents [31], mesoporous MgO [28,32,33], mesoporous MgO/TiO_2 mixed oxides [34], and mesoporous MgO/carbon composites [35]. However, the synthesis processes for these sorbents are time consuming, involve multistep procedures, use a template and/or need toxic solvents [36]. The other way to improve sorption capacity is to add a "promoter". Particularly, alkali-metal carbonates such as K_2CO_3 have been widely used to enhance the sorption capacity and to tune the sorption temperatures [27,37–40]. Other promoters have seldom been reported [41].

In this work, Al_2O_3 and CeO_2 were added as promoters to enhance the CO_2 capture capacity of MgO sorbents at moderate temperatures. In order to increase the surface area and porosity of MgO, a urea-co-precipitation method which was previously used to prepare mesoporous TiO_2-CeO_2 adsorbents for deep desulfurization [42] was adopted. The prepared MgO-based sorbents were characterized by N_2 physisorption, X-ray powder diffraction (XRD) and scanning electron microscopy (SEM). Their CO_2 sorption performances were evaluated using CO_2 temperature programmed desorption (TPD) experiments. The effects of the amounts of Al_2O_3 and CeO_2 added, and the sorption temperatures were studied. The regenerability and cyclic stability of the promoted MgO sorbents was also examined.

2 Experimental

2.1 Materials

Magnesium nitrate hexahydrate ($Mg(NO_3)_2 \cdot 6H_2O$, ACS reagent, 99%), alumina nitrate nonahydrate ($Al(NO_3)_3 \cdot 9H_2O$, ACS reagent, ⩾98%), ammonium cerium nitrate ($(NH_4)_2Ce(NO_3)_6$, ACS reagent, ⩾98.5%) and urea ($CO(NH_2)_2$, ACS reagent, 99.0%–100.5%) were purchased from Sigma-Aldrich and used as received. The gases, ultra-high purity (UHP) nitrogen (99.999%), Coleman grade CO_2 (99.99%) and UHP helium (99.999%), for N_2 physisorption analysis and CO_2 sorption-desorption were purchased from Praxair, USA.

2.2 Sorbents preparation

The MgO-based sorbents including pure MgO, Al_2O_3 promoted MgO, CeO_2 promoted MgO, pure Al_2O_3, and pure CeO_2 were prepared by a modified urea co-precipitation method on the basis of the procedure reported by Watanabe et al. [42]. First the required aqueous solutions were prepared using magnesium nitrate hexahydrate, alumina nitrate nonahydrate, ammonium cerium nitrate and urea. The aqueous nitrate solutions (1 mol/L) were mixed and added to the urea solution (1.6 mol/L). The mixture was then heated to 95 °C and kept at this temperature for 2 h under stirring. During the course ammonia water (~37%) was added to the mixture drop by drop to adjust the pH value to 11.6. The resultant white precipitant was filtered, dried overnight and then calcined in a muffle finance at 450 °C for 2 h at a heating rate of 2 °C/min. The synthesis procedure for the pure Al_2O_3 and CeO_2 samples was the same as described above.

2.3 Characterizations

The prepared sorbents were characterized by N_2 physisorption, XRD and SEM. N_2 physisorption was carried out at −196 °C on a Micromeritics ASAP 2020 surface area and porosity analyzer, from which the Brunauer-Emmett-Teller (BET) surface areas, the pore volumes and the pore sizes were obtained. All samples were degassed at 220 °C prior to the N_2 adsorption-desorption measurements. The pore volumes were calculated from the adsorbed nitrogen after complete pore condensation at the relative pressure of P/P_0 = 0.995. The pore sizes were estimated from the desorption branch using the Barrett-Joyner-Halenda (BJH) method.

XRD patterns were collected in the 2θ range from 10°–90° using a Bruker D8 Advance X-ray diffractometer equipped with Cu Kα radiation (λ = 0.154 nm). The working voltage of the instrument was 40 kV and the current was 40 mA. The diffractograms were analyzed using MDI JADE 8.0 software and standard JCPDS files. The SEM images of the synthesized samples were collected with a FEI Magellan 400 instrument operated at 5 kV, in conjunction with energy dispersive X-ray spectroscopy (EDS).

2.4 CO_2 sorption evaluation

The CO_2 sorption performance of the sorbents was evaluated using CO_2 temperature programmed desorption (TPD) performed on a Micromeritics AutoChem 2910 instrument equipped with a thermal conductive detector (TCD). In a typical CO_2-TPD test, about 200 mg of sorbent sample was loaded into a U-shaped quartz tube and pretreated at 400 °C under a helium flow for 20 min. The temperature was then reduced to the desired temperature and the CO_2 sorption was conducted by flowing pure CO_2 through the sample at 20 mL/min for 30 min. Then the temperature was decreased to 50 °C under the same CO_2 flow. The desorption experiment was performed by purging helium gas (20 mL/min) through the sorbent bed and ramping the temperature from 50 to 400 °C at a rate of 10 °C/min. The temperature was then held at 400 °C for 20 min to complete the desorption. The CO_2 sorption capacity was calculated in mg CO_2 per g of sorbent (mg-CO_2/g-S) using the amount of CO_2 desorbed which was obtained from the desorption curve recorded by the on-line TCD. The TCD signal was calibrated by using a known amount of CO_2. Moderate temperatures of 50, 100, 150, 200, 250, 300 and 350 °C were examined.

3 Results and discussion

3.1 Effect of Al_2O_3 and CeO_2 loadings

Table 1 shows the effect of Al_2O_3 and CeO_2 loadings on the CO_2 capacity of the MgO sorbents. For comparison, pure MgO, Al_2O_3 and CeO_2 prepared via the same procedure were also evaluated. At a sorption temperature of 200 °C, the pure metal oxides all had similar capacities for CO_2 sorption, i.e., 12.9, 12.3 and 12.7 mg-CO_2/g-S for pure MgO, Al_2O_3 and CeO_2 respectively. The capacity of the MgO sorbent prepared in this work is slightly better than that of the non-porous MgO (9.0 mg-CO_2/g-S) reported in the literature [28,43].

The addition of any amount of Al_2O_3 or CeO_2 resulted in higher sorption capacities than those obtained for any of the pure sorbents (Table 1). The Al_2O_3-MgO sorbent had a maximum capacity of 20.1 mg-CO_2/g-S when the Mg/Al molar ratio was 3, which is about 56% higher than that of pure MgO. Similarly the CeO_2 modified MgO had a maximum CO_2 capacity of 35.3 mg-CO_2/g-S with a Mg/Ce molar ratio of 3. This capacity is about two times higher than those of pure MgO and CeO_2. For any given ratio of Mg/Al(Ce), the CeO_2-MgO always had a higher capacity than the Al_2O_3-MgO sorbents so CeO_2 is a better promoter to improve the sorption capacity of MgO.

Table 1 CO_2 sorption capacity of pure MgO, Al_2O_3, CeO_2 and Al_2O_3- and CeO_2-pormoted MgO sorbents[a)]

Sample	Mg/M molar ratio	T/°C	CO_2 capacity /(mg-CO_2·g-S^{-1})	Ref.
MgO	–	200	12.9	This study
Al_2O_3-MgO	9	200	15.9	This study
	3		20.1	
	1		17.0	
	1/3		14.9	
Al_2O_3	–	200	12.3	This study
CeO_2-MgO	9	200	18.2	This study
	3		35.3	
	1		24.8	
	1/3		19.5	
CeO_2	–	200	12.7	This study
MgO	–	200	9.0	[43]
MgO/γ-Al_2O_3	1.4	200	37	[43]
γ-Al_2O_3	–	200	6.0	[43]
MgO/Al_2O_3	0.14	150	21.6	[31]
Mg-Al HTlc	1.8	200	10.6	[44]
Mg-Al HTlc	2.1	200	5.3	[44]
Mg-Al HTlc	3.2	200	36.5	[45]
MgO-ZrO_2	0.5	150	44.4	[46]

[a)] Measured by CO_2-TPD with CO_2 sorption at 200 °C

Modified MgO adsorbents have also been reported by other researchers [31,43–46], and these are also summarized in Table 1. Han et al. synthesized a MgO/γ-Al_2O_3 composite with a Mg/Al ratio of 1.4 which exhibited a much higher CO_2 adsorption capacity (37 mg-CO_2/g-S) than MgO (9 mg-CO_2/g-S) and γ-Al_2O_3 (6 mg-CO_2/g-S) at 200 °C under atmospheric pressure [43]. A capacity of 21.6 mg-CO_2/g-S over a MgO/Al_2O_3 adsorbent (Mg/Al = 0.14) at 150 °C has also been reported by Li et al. [31]. A CO_2 capacity of 44.4 mg-CO_2/g-S was obtained over MgO/ZrO_2 (Mg/Zr = 0.5) at 150 °C [46]. Another type of moderate-temperature-CO_2 adsorbents is hydrotalcite (HTlc)-like compounds which contain both MgO and Al_2O_3. The CO_2 capacities for Mg-Al HTlc at 200 °C varied between 5–37 mg-CO_2/g-S for Mg/Al ratios between 1.8–3.2 [44,45]. Thus, the Al_2O_3 and CeO_2-modified MgO sorbents in this work have either higher or comparable CO_2 sorption capacities to those reported in the literature.

3.2 Sorbent characterizations

Surface area and the basic properties of sorbent materials are both critical factors affecting their CO_2 sorption capacities because the larger surface area could provide more sites and the basicity could increase the affinity of the sites for CO_2 sorption. Thus, in order to understand the promotion effect of Al_2O_3 and CeO_2 on the sorption capacity of MgO, various characterizations were carried out. Nitrogen physisorption experiments were conducted to determine the porous properties, XRD was used to elucidate texture and composition, SEM was employed to determine morphologies, and CO_2-TPD was used to determine the basicity of the sorbent materials. Since the Mg/Al(Ce) molar ratios of 3 gave the best results, these samples were selected for the characterization studies.

3.2.1 N_2 physisorption

The N_2 adsorption-desorption isotherms for the Al_2O_3-MgO and CeO_2-MgO samples are shown in Fig. 1. The isotherms of pure MgO, Al_2O_3 and CeO_2 are also presented for comparison. The pure MgO has a type-II adsorption isotherm and the hysteresis loop is located at high relative P/P_0, suggesting that the prepared MgO sorbent contains mainly macropores [47]. The isotherms for the pure Al_2O_3 and CeO_2 samples are mixed type-II and type-IV, suggesting that the Al_2O_3 and CeO_2 samples prepared from the co-precipitation method contain both mesopores and macropores. However, over the Al_2O_3-pomoted MgO sample, a typical type-IV adsorption isotherm with a H2 hysteresis loop was obtained, indicating a uniform meso-structure. Watanabe et al. also observed a mesoporous structure for mixed TiO_2-CeO_2 oxides prepared via a similar method [42]. The CeO_2-MgO sorbent also exhibited a type-IV adsorption isotherm, but with a H3 hysteresis loop, suggesting that it has larger mesopores and that the pores are not as uniform as those in the Al_2O_3-MgO sample.

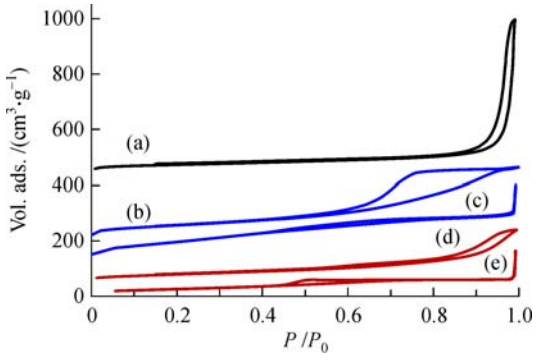

Fig. 1 N_2 adsorption isotherms of (a) pure MgO, (b) Al_2O_3-MgO, (c) Al_2O_3, (d) CeO_2-MgO and (e) CeO_2

The surface areas, pore volumes and pore sizes were calculated from the N_2 adsorption isotherms and the results are listed in Table 2. The pore size distribution curves for each sample were obtained using the BJH method and are shown in Fig. 2. MgO had a surface area of 83 m^2/g with large pore volume of 0.84 cm^3/g and a pore size of about 60 nm. Thus, the higher CO_2 sorption capacity of MgO sorbent compared to the non-porous MgO reported in literature [28] can be attributed to its high surface area and porous structure. Pure Al_2O_3 showed the highest surface area of 284 m^2/g with a narrow pore distribution centered at ca. 6.0 nm. Pure CeO_2 had a surface area of 96 m^2/g with a broad pore size distribution.

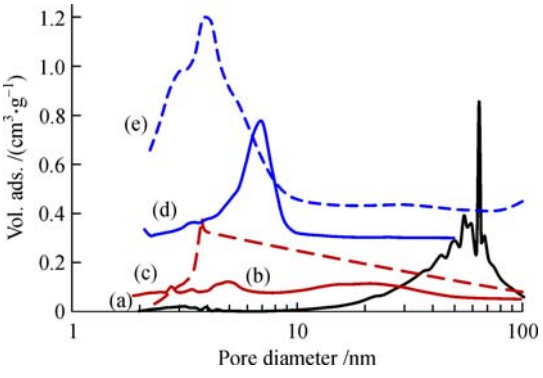

Fig. 2 The BJH pore size distribution curves for (a) pure MgO, (b) CeO_2-MgO, (c) CeO_2, (d) Al_2O_3-MgO and (e) Al_2O_3

After the addition of Al_2O_3, the Al_2O_3-MgO sample showed a narrow pore distribution centered at 6.0 nm and it had a high surface area of 200 m^2/g which is more than twice that of pure MgO. With the addition of CeO_2, the CeO_2-MgO had a surface area of about 107 m^2/g which is

Table 2 The porous properties of MgO, Al_2O_3, CeO_2, Al_2O_3-MgO and CeO_2-MgO

Sample	S_{BET} /($m^2 \cdot g^{-1}$)	Pore volume/ ($cm^3 \cdot g^{-1}$)	Pore size[a)]/nm	MgO crystallite size[b)]/nm
MgO	83	0.84	59.5	14.3±1.1
Al_2O_3	284	0.47	3.8	–
CeO_2	96	0.27	3.7	–
Al_2O_3-MgO (1:3)	200	0.41	7.0	4.9±0.3
CeO_2-MgO (1:3)	107	0.30	4.9	13.6±1.2

a) Data from the BJH pore size distribution curves shown in Fig. 2; b) calculated from MgO (200) reflection using the Scherrer equation

significantly less than that of Al_2O_3-MgO but higher than that of either MgO or CeO_2 alone. The pore size distribution of CeO_2-MgO is narrower than pure CeO_2, but much broader than Al_2O_3-MgO. Based on these results, it can be deduced that the improved surface area and mesoporous structure of MgO could be one reason for the improved CO_2 sorption capacity of the MgO sorbent after the addition of Al_2O_3 or CeO_2. This is in agreement with the observations reported by other researchers [28,31–34]. However, it should be noted that although the Al_2O_3-MgO had a higher surface area, a larger pore volume and a more uniform pore structure than CeO_2-MgO, its CO_2 sorption capacity was lower (Table 1). This indicates that besides the pore properties, other factors such as MgO crystallite size and basicity may also affect the CO_2 sorption capacity of the promoted MgO sorbents.

3.2.2 XRD

Figure 3 shows the XRD patterns of the Al_2O_3- and CeO_2-promoted MgO sorbents along with the pure MgO, Al_2O_3 and CeO_2 samples. The XRD patterns of the MgO, Al_2O_3 and CeO_2 samples have the diffraction peaks that can be indexed to crystalline MgO (JCPDS 78-0430), γ-Al_2O_3 (JCPDS 10-0425) and CeO_2 (JCPDS 34-0394), respectively. In the XRD pattern of the bimetal oxide Al_2O_3-MgO, no γ-Al_2O_3 peaks are detected and the MgO diffraction peaks are lower and wider than those in the pure MgO sample. This suggests that the loaded Al_2O_3 is highly dispersed and incorporated in the MgO bulk which would result in the higher surface area compared to the pure MgO as observed in the N_2 physisorption data (Table 2). In contrast, for the CeO_2-MgO sample, crystal phases for both MgO and CeO_2 are seen, because a large amount of CeO_2 was added (At the Mg/Ce molar ratio of 3, the CeO_2 mass content of CeO_2-MgO is about 59 wt-%.). The diffraction intensities for the MgO phase are much lower than those in either pure MgO or Al_2O_3-MgO, indicating that MgO might be highly dispersed over the surface of CeO_2.

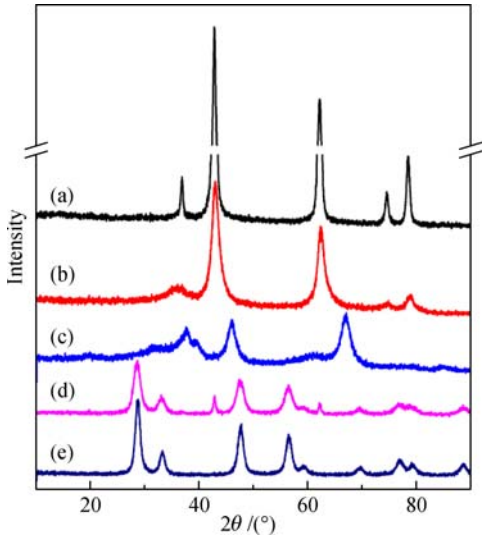

Fig. 3 XRD patterns of (a) pure MgO, (b) Al_2O_3-MgO, (c) Al_2O_3, (d) CeO_2-MgO and (e) CeO_2

The mean MgO crystallite sizes were calculated from the peak widths of the XRD peaks using the Scherrer equation [48]:

$$t = K\lambda/(\beta\cos\theta),$$

where t is the mean crystallite size, λ is the wavelength of the radiation (Cu, K_α), β is the full-width at half maximum of the diffraction peak (in rad.), θ is the Bragg's angle and K is particle shape factor which is taken to be 0.85. The estimated MgO crystallite sizes based on the MgO (200) reflection are given in Table 2. The pure MgO had a crystallite size of 14.3 nm. The addition of Al_2O_3 caused a significant reduction in the MgO crystallite size to about 4.9 nm. But the addition of CeO_2 only produced a small decrease in the MgO crystallite size (13.6 nm). Based on these results, another reason for the improved CO_2 sorption capacity of the Al_2O_3- and CeO_2-promoted MgO sorbents may be the greatly reduced MgO crystallite size and the improved dispersion of MgO crystals with the addition of Al_2O_3 and CeO_2, respectively.

3.2.3 SEM-EDS

Figure 4 shows the SEM images and EDS results for the MgO, Al_2O_3-MgO and CeO_2-MgO samples. The pure MgO is composed of stacked blocks ranging in size from 20–50 nm with pores between the stacked blocks. With the addition of Al_2O_3, the morphology of the Al_2O_3-MgO sample changed to stacked rods and the particle sizes became more homogeneous with sizes less than 20 nm. In addition, a larger network of pores is observed. The morphology of CeO_2-MgO is similar to that of the pure MgO, except that the particles are smaller (mainly below 20 nm) and the porosity is higher with more nanopores and open voids presented between particles than MgO (Fig. 4(c) *vs.* 4(a)). The SEM observations are consistent with the results from the N_2 adsorption isotherms and XRD analysis.

EDS provides information about the elemental composition of materials. As expected, the pure MgO contained 100 wt-% MgO as shown in Fig. 4(a). The Al_2O_3-MgO and CeO_2-MgO samples are composed of 68 wt-% MgO-32 wt-% Al_2O_3, and 41 wt-% MgO-59 wt-% CeO_2, respectively (Figs. 4(b) and 4(c)). That is, the molar ratios of Mg/Al and Mg/Ce were 2.72 and 2.95, respectively for the Al_2O_3-MgO and CeO_2-MgO samples. This verifies that the mixed oxide samples were prepared according to the experimental design with molar ratios of 3.0.

The distributions of MgO and CeO_2 (or Al_2O_3) in CeO_2-

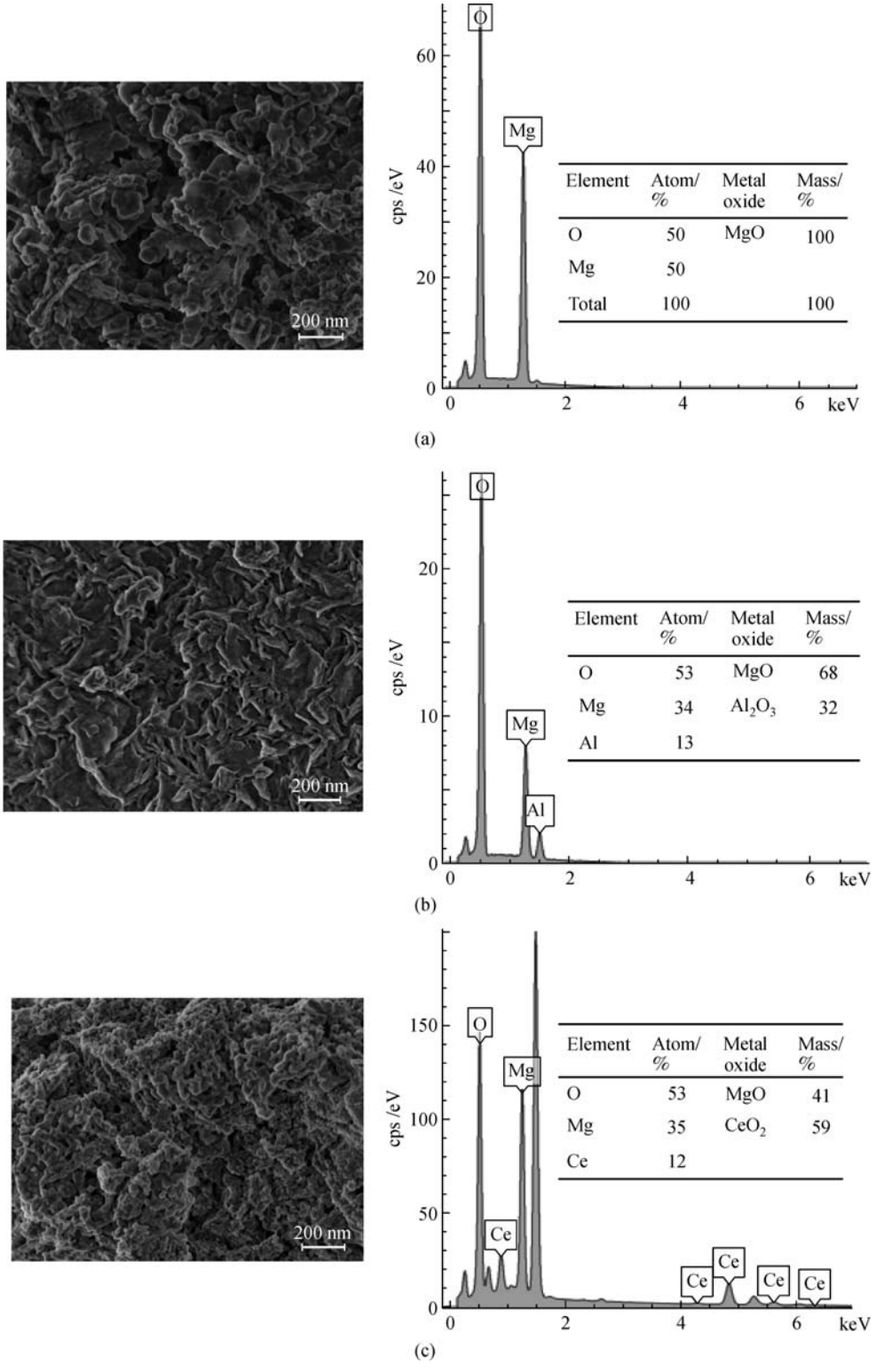

Fig. 4 SEM and EDS results for (a) pure MgO, (b) Al_2O_3-MgO and (c) CeO_2-MgO

MgO (or Al_2O_3-MgO) were further examined by X-ray elemental mapping analysis and the results are shown in Fig. 5. In these images red represents Ce (or Al), green is Mg and blue is O. From Fig. 5(a), it can be seen that there is an uneven distribution of Mg and Ce in CeO_2-MgO. Small particles are stacked together forming a big sphere-like particle. Ce is located outside, covering Mg underneath, as illustrated in Fig. 5(a) with considering the distributions of Mg and Ce showed in the insets. In contrast, the distribution of Mg and Al is highly uniform in Al_2O_3-MgO (Fig. 5(b)).

3.2.4 CO_2-TPD

For MgO-based sorbents, the basicity is also a key factor that influences the CO_2 sorption capacity. So the basicity of the pure MgO, Al_2O_3-MgO and CeO_2-MgO was evaluated by CO_2-TPD and the results are shown in Fig. 6. The CO_2 sorption was conducted at 200 °C by flowing pure CO_2 at a flow rate of 20 mL/min for 20 min. In consideration of moderate temperature applications, the desorption temperature was set at 400 °C. For pure MgO, the desorption started at about 70 °C and reached a peak at 248 °C (Fig. 6 (a)). The addition of Al_2O_3 caused a slight shift in the desorption curve and the desorption did not start until the temperature was over 100 °C (Fig. 6(b)). The desorption peak occurred at 251 °C, which is very close to that for pure MgO. This implies that the basicity strength of the Al_2O_3-MgO sorbent is almost the same as that of the pure MgO. In the range of 50–150 °C, the desorption behavior of CeO_2-MgO was similar to that for the pure MgO (Fig. 6(c)). However at temperatures over 150 °C, the CO_2 desorbed more quickly and peaked at 260 °C, which is 10 °C higher than the other two samples. A higher desorption temperature implies that the interaction between the MgO and CO_2 became stronger. In other words, the basicity of the MgO is improved with the addition of CeO_2, and this can also contribute to the better CO_2 sorption capacity of CeO_2-MgO compared to Al_2O_3-MgO and pure MgO.

Recently a MgO modified zeolite was prepared for CO_2 capture [49]. This material had an isosteric adsorption heat of about 47 kJ/mol which is much lower than the reaction enthalpy shown in Eq. (1). However this value is comparable with those reported for other alkali-metal exchanged low-silica zeolites such as NaY and CsY (40–50 kJ/mol) [50]. A mesoporous carbon nitride material, MCN-8E-150, has a similar isosteric adsorption heat (35–53 kJ/mol) for CO_2 [51]. The isosteric heat of adsorption is usually used to characterize the strength of the interactions between CO_2 and zeolite adsorbents. So, such a low value for the MgO modified zeolite indicates that CO_2 is mainly adsorbed on the internal surface within the zeolite pore structure rather than on the MgO particles, especially at low MgO loadings (0.8–1.5 wt-%) [49].

The addition of Al_2O_3 and CeO_2 also resulted in much larger desorption peaks than that for pure MgO. The amount of desorbed CO_2 calculated from the desorption peak was 20.1 and 35.3 mg-CO_2/g-S for Al_2O_3-MgO and CeO_2-MgO, respectively, higher than 12.9 mg-CO_2/g-S for pure MgO. At 200 °C, the CO_2 sorption can be reasonably considered to occur as a chemical reaction between MgO and CO_2. Thus, the amount of desorbed CO_2 per gram of MgO is indicative of the activity of the MgO phase in the sorbent. Based on the weight percentages estimated from the SEM-EDS results, this value for the Al_2O_3-MgO sample is 29.5 mg-CO_2/g-MgO which is more than double of that for the pure MgO sample (12.9 mg-CO_2/g-MgO). The value for CeO_2-MgO is even larger, 86.7 mg-CO_2/g-MgO, almost three times that for the Al_2O_3-MgO and more than six times that for the pure MgO. Therefore, the addition of either Al_2O_3 or CeO_2 makes MgO more active for CO_2 sorption and CeO_2 has a much larger promotion effect than Al_2O_3.

3.3 Effect of sorption temperature

The effect of the sorption temperature on the CO_2 sorption

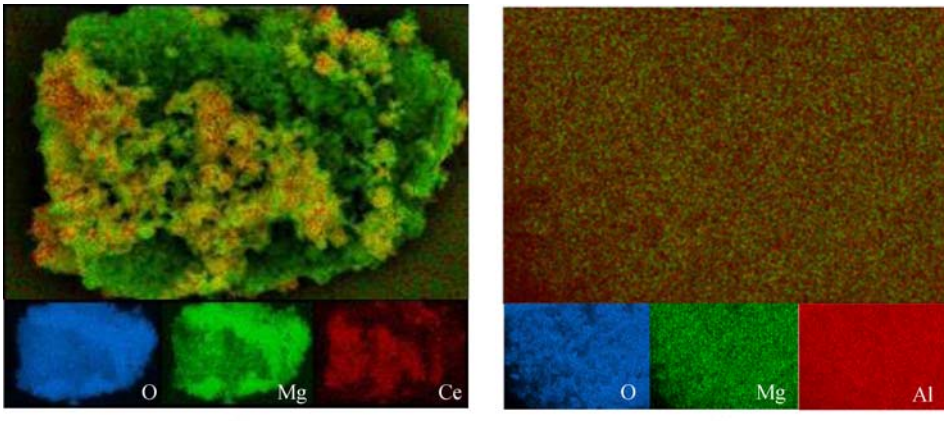

Fig. 5 SEM X-ray elemental mapping images of (a) CeO_2-MgO and (b) Al_2O_3-MgO

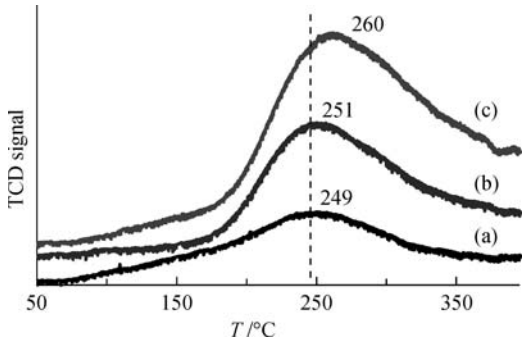

Fig. 6 CO_2-TPD profiles of (a) pure MgO, (b) Al_2O_3-MgO and (c) CeO_2-MgO samples. CO_2 sorption was conducted at 200 °C with pure CO_2 flow at 20 mL/min for 20 min

was examined using various moderate temperatures including 50, 100, 150, 200, 250, 300 and 350 °C with 100% CO_2 at 20 mL/min. Figure 7 shows the CO_2 uptake measured by CO_2-TPD as a function of sorption temperature over pure MgO, Al_2O_3-MgO and CeO_2-MgO. For MgO, the best CO_2 capacity of 15.3 mg-CO_2/g-S was obtained at 100 °C. The Al_2O_3-MgO sorbent had a similar temperature-dependent CO_2 sorption trend and its best capacity (24.6 mg-CO_2/g-S) was also achieved at 100 °C. However, the Al_2O_3-MgO sorbent had higher CO_2 capacities than the unmodified MgO sorbent at all temperatures. The higher capacity of the Al_2O_3-MgO sorbent can be attributed to the increased surface area with better MgO dispersion and smaller MgO particle sizes.

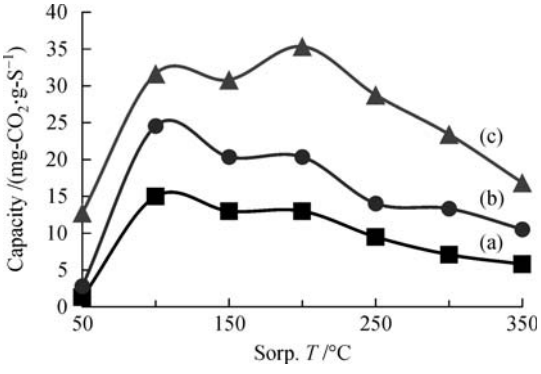

Fig. 7 CO_2 uptake measured by CO_2-TPD as a function of sorption temperature over (a) pure MgO, (b) Al_2O_3-MgO and (c) CeO_2-MgO

The CeO_2 promoted MgO sorbent exhibited a similar temperature trend and the capacities were much higher than those of either pure MgO or Al_2O_3-MgO at all temperatures. The highest capacity (35.3 mg-CO_2/g-S) was obtained at 200 °C, which is 100 °C higher than the maximum for the other two sorbents. The shift of the optimum sorption temperature is due to the improved MgO basicity induced by the incorporation of CeO_2 as shown in the CO_2-TPD results (Fig. 6). The maximum capacity of 35.3 mg-CO_2/g-S is about 171% and 74% higher than those for the pure MgO and Al_2O_3-MgO at 200 °C, respectively.

Since the surface areas of CeO_2-MgO and pure MgO are similar, the increased CO_2 capacity can be ascribed to the change in the pore structures and the increase in the basicity of the MgO phase induced by the addition of CeO_2. Since Al_2O_3-MgO showed a much higher surface area (Table 2) but a lower CO_2 capacity than CeO_2-MgO under the same conditions, it can be concluded that the improvement in the sorbent structure and the basicity of the MgO phase is more important than the increase in the surface area for enhancing the CO_2 sorption capacity of MgO-based sorbents.

3.4 Regenerability and stability

To be useful for practical applications, a sorbent should not only possess a high capacity but also have excellent regenerability and stable performance for multiple sorption-desorption cycles. Figure 8 shows the CO_2 sorption capacities of the pure MgO, Al_2O_3-MgO and CeO_2-MgO sorbents as a function of sorption-desorption cycles. The CO_2 sorption was performed at 100 °C for pure MgO and Al_2O_3-MgO and at 200 °C for CeO_2-MgO using a flow of pure CO_2 and the desorption was conducted at 400 °C under helium. During the 15 sorption-desorption cycles, the CO_2 capacity over the pure MgO sorbent exhibited a monotonic decrease. The capacity drop was about 20% after 15 cycles. For the Al_2O_3-MgO and CeO_2-MgO sorbents, a fairly large drop in the capacity was observed during the first six cycles but then the capacity became more stable with extended cycles. The capacity drop after the first six cycles was 3.8% for Al_2O_3-MgO and 9.6% for CeO_2-MgO, less than 14.1% for MgO. The CO_2 capacity in the last five cycles was 17.5, 17.6, 18.2, 17.9, 17.9 mg-CO_2/g-S for the Al_2O_3-MgO sorbent and 24.1, 23.7, 23.5, 23.3 and 23.5 mg-CO_2/g-S for the CeO_2-MgO sorbent,

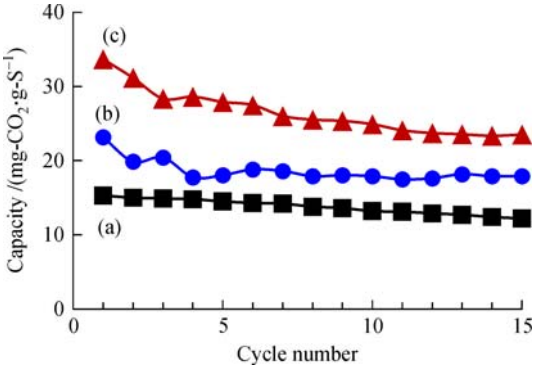

Fig. 8 CO_2 capacity measured by CO_2-TPD as a function of sorption-desorption cycles over (a) pure MgO, (b) Al_2O_3-MgO and (c) CeO_2-MgO

respectively. Thus the MgO, Al_2O_3-MgO and CeO_2-MgO sorbents are regenerable and retain more than 70% of their initial CO_2 capacity at a moderate regeneration temperature of 400 °C. Furthermore, the addition of Al_2O_3 or CeO_2 to MgO improved the cyclic stability of the MgO sorbent, especially at the elongated operation.

The morphologies of the spent MgO, Al_2O_3-MgO and CeO_2-MgO sorbents after 15 cycles of CO_2 sorption-desorption were examined by SEM and are shown in Fig. 9. The morphology of the spent MgO sorbent changed a great deal compared to the fresh sorbent (Fig. 4). The particles are much larger which may explain the decrease in the capacity of the pure MgO sorbent with sorption-desorption cycles. In contrast, the morphologies of the spent Al_2O_3-MgO and CeO_2-MgO sorbents hardly changed, indicating the addition of Al_2O_3 and CeO_2 improved the sintering resistance of MgO. As a result, Al_2O_3-MgO and CeO_2-MgO sorbents exhibited the better stabilities in cyclic CO_2 capture at moderate temperatures.

4 Conclusions

A series of MgO-based sorbents was prepared by a urea co-precipitation method and the promotion effect of Al_2O_3 and CeO_2 on the CO_2 sorption capacity of the MgO sorbent was studied. The addition of Al_2O_3 and CeO_2 improved the CO_2 capacity of the MgO sorbent and the best molar ratios for both Mg/Al and Mg/Ce were 3. The effect of the sorption temperature was also investigated. Over pure MgO, the best capacity of 15.3 mg-CO_2/g-S was obtained at a sorption temperature of 100 °C. The best capacity for the Al_2O_3-MgO sorbent was 24.6 mg-CO_2/g-S which was also obtained at 100 °C. The CeO_2-MgO sorbent had the highest sorption capacity of 35.3 mg-CO_2/g-S and its optimal temperature was 200 °C. The characterizations showed that the higher capacity of the Al_2O_3-MgO sorbent can be attributed mainly to the increased surface area with better MgO dispersion and smaller MgO crystallites. In the case of CeO_2 addition, the increased CO_2 capacity can be ascribed to the changes in the structure and the increase in the basicity of the MgO phase. These results demonstrate that CeO_2 is more effective for promoting the CO_2 sorption capacity of MgO than Al_2O_3, and the increase in the basicity is more important than the increase in the surface area to enhance the sorption capacity of the MgO sorbent. The Al_2O_3-MgO and CeO_2-MgO sorbents are regenerable for CO_2 sorption under a moderate temperature and both exhibited better cyclic stability than the pure MgO sorbent.

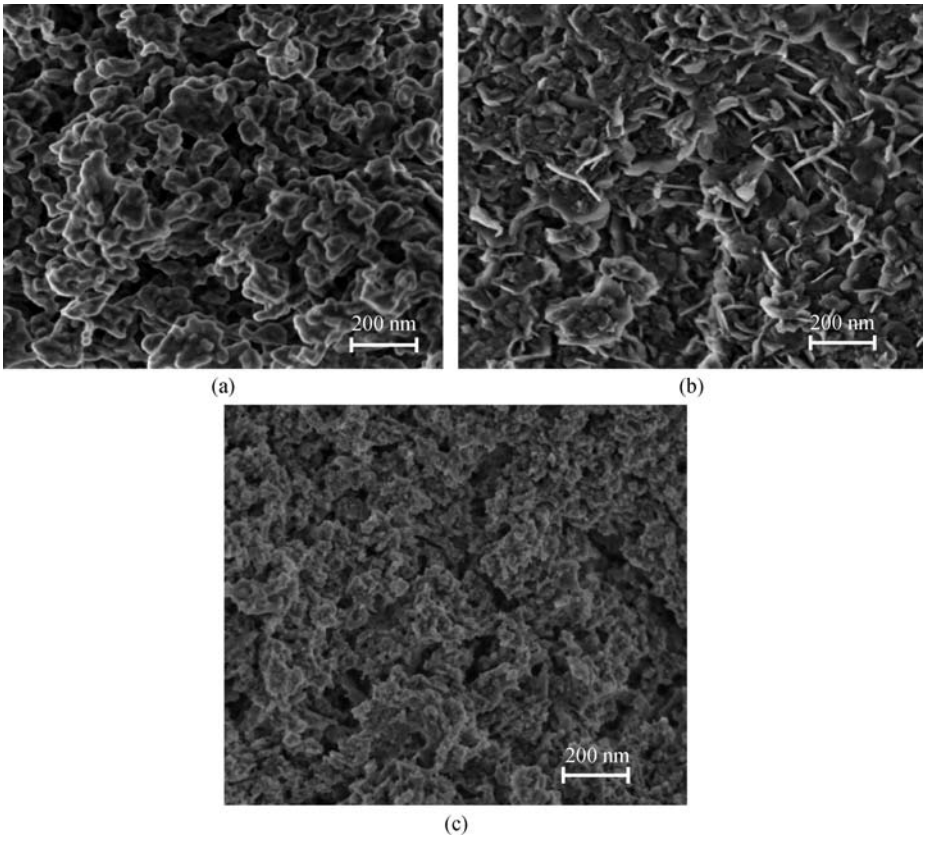

Fig. 9 SEM images of (a) spent MgO, (b) spent Al_2O_3-MgO and (c) spent CeO_2-MgO sorbents after 15 cycles of CO_2 sorption-desorption

Acknowledgements The authors gratefully acknowledge the financial support from Pennsylvania State University through the Penn State Institutes of Energy and the Environment, and from the National Natural Science Foundation of China (Grant No. 21005083) and the Innovative Fund of Shanghai Institute of Ceramics, Chinese Academy of Sciences (Grant No. Y37ZC4140G). Dr. Huimei Yu would like to thank the Chinese Academy of Sciences for the visiting scholarship and Dr. Song for the visiting scholar invitation to the EMS Energy Institute at Penn State.

References

1. Williams J H, De Benedictis A, Ghanadan R, Mahone A, Moore J, Morrow W R, Price S, Torn M S. The technology path to deep greenhouse gas emissions cuts by 2050: The pivotal role of electricity. Science, 2012, 335(6064): 53–59
2. Ma X L, Wang X X, Song C S. "Molecular basket" sorbents for separation of CO_2 and H_2S from various gas streams. Journal of the American Chemical Society, 2009, 131(16): 5777–5783
3. Song C S. Global challenges and strategies for control, conversion and utilization of CO_2 for sustainable development involving energy, catalysis, adsorption and chemical processing. Catalysis Today, 2006, 115(1-4): 2–32
4. Sema T, Naami A, Liang Z W, Shi H C, Layer A V, Sumon K Z, Wattanaphan P, Henni A, Idem R, Saiwan C, Tontiwachwuthikul P. Part 5b: Solvent chemistry: Reaction kinetics of CO_2 absorption into reactive amine solutions. Carbon Management, 2012, 3(2): 201–220
5. Wilson M, Tontiwachwuthikul P, Chakma A, Idem R, Veawab A, Aroonwilas A, Gelowitz D, Barrie J, Mariz C. Test results from a CO_2 extraction pilot plant at boundary dam coal-fired power station. Energy, 2004, 29(9-10): 1259–1267
6. Krull F F, Fritzmann C, Melin T. Liquid membranes for gas/vapor separation. Journal of Membrane Science, 2008, 325(2): 509–519
7. Aaron D, Tsouris C. Separation of CO_2 from flue gas: A review. Separation Science and Technology, 2005, 40(1-3): 321–348
8. Meratla Z. Combining cryogenic flue gas emission remediation with a CO_2/O_2 combustion cycle. Energy Conversion and Management, 1997, 38: S147–S152
9. D'Alessandro D M, Smit B, Long J R. Carbon dioxide capture: Prospects for new materials. Angewandte Chemie International Edition, 2010, 49(35): 6058–6082
10. Sevilla M, Fuertes A B. CO_2 adsorption by activated templated carbons. Journal of Colloid and Interface Science, 2012, 366(1): 147–154
11. Chen Z H, Deng S B, Wei H R, Wang B, Huang J, Yu G. Activated carbons and amine-modified materials for carbon dioxide capture—a review. Frontiers of Environmental Science & Engineering, 2013, 7(3): 326–340
12. Du T, Liu L Y, Xiao P, Che S, Wang H M. Preparation of zeolite NaA for CO_2 capture from nickel laterite residue. International Journal of Minerals Metallurgy and Materials, 2014, 21: 820–825
13. Torrisi A, Bell R G, Mellot-Draznieks C. Functionalized MOFs for enhanced CO_2 capture. Crystal Growth & Design, 2010, 10(7): 2839–2841
14. Gonzalez-Zamora E, Ibrra I A. CO_2 capture under humid conditions in metal-organic frameworks. Materials Chemistry Frontiers, 2017, 1(8): 1471–1484
15. Razavi S S, Hashemianzadeh S M, Karimi H. Modeling the adsorptive selectivity of carbon nanotubes for effective separation of CO_2/N_2 mixtures. Journal of Molecular Modeling, 2011, 17(5): 1163–1172
16. Simmons J M, Wu H, Zhou W, Yildirim T. Carbon capture in metal-organic frameworks—a comparative study. Energy & Environmental Science, 2011, 4(6): 2177–2185
17. Xu X C, Song C S, Andresen J M, Miller B G, Scaroni A W. Novel polyethylenimine-modified mesoporous molecular sieve of MCM-41 type as high-capacity adsorbent for CO_2 capture. Energy & Fuels, 2002, 16(6): 1463–1469
18. Choi S, Drese J H, Jones C W. Adsorbent materials for carbon dioxide capture from large anthropogenic point sources. ChemSusChem, 2009, 2(9): 796–854
19. Darunte L A, Walton K S, Sholl D S, Jones C W. CO_2 capture via adsorption in amine-functionalized sorbents. Current Opinion in Chemical Engineering, 2016, 12: 82–90
20. Sayari A, Heydari-Gorji A, Yang Y. CO_2-induced degradation of amine-containing adsorbents: Reaction products and pathways. Journal of the American Chemical Society, 2012, 134(33): 13834–13842
21. Sayari A, Belmabkhout Y. Stabilization of amine-containing CO_2 adsorbents: Dramatic effect of water vapor. Journal of the American Chemical Society, 2010, 132(18): 6312–6314
22. Wang K, Wang X Y, Zhao P F, Guo X. High-temperature capture of CO_2 on lithium-based sorbents prepared by a water-based sol-gel technique. Chemical Engineering & Technology, 2014, 37(9): 1552–1558
23. Chen H C, Zhang P P, Duan Y F, Zhao C S. Reactivity enhancement of calcium based sorbents by doped with metal oxides through the sol-gel process. Applied Energy, 2016, 162: 390–400
24. Wang S P, Fan S S, Zhao Y J, Fan L J, Liu S Y, Ma X B. Carbonation condition and modeling studies of calcium-based sorbent in the fixed-bed reactor. Industrial & Engineering Chemistry Research, 2014, 53(25): 10457–10464
25. Zhao Y, Han Y H, Ma T Z, Guo T X. Simultaneous desulfurization and denitrification from flue gas by ferrate(VI). Environmental Science & Technology, 2011, 45(9): 4060–4065
26. Wang M, Lawal A, Stephenson P, Sidders J, Ramshaw C. Post-combustion CO_2 capture with chemical absorption: A state-of-the-art review. Chemical Engineering Research & Design, 2011, 89(9): 1609–1624
27. Liu M Y, Vogt C, Chaffee A L, Chang S L Y. Nanoscale structural investigation of Cs_2CO_3-doped MgO sorbent for CO_2 capture at moderate temperature. Journal of Physical Chemistry C, 2013, 117 (34): 17514–17520
28. Li Y Y, Han K K, Lin W G, Wan M M, Wang Y, Zhu J H. Fabrication of a new MgO/C sorbent for CO_2 capture at elevated temperature. Journal of Materials Chemistry. A, Materials for Energy and Sustainability, 2013, 1(41): 12919–12925
29. Liu W J, Jiang H, Tian K, Ding Y W, Yu H Q. Mesoporous carbon stabilized MgO nanoparticles synthesized by pyrolysis of $MgCl_2$ preloaded waste biomass for highly efficient CO_2 capture. Environmental Science & Technology, 2013, 47(16): 9397–9403
30. Zukal A, Pastva J, Cejka J. MgO-modified mesoporous silicas impregnated by potassium carbonate for carbon dioxide adsorption.

Microporous and Mesoporous Materials, 2013, 167: 44–50
31. Li L, Wen X, Fu X, Wang F, Zhao N, Xiao F K, Wei W, Sun Y H. MgO/Al_2O_3 sorbent for CO_2 capture. Energy & Fuels, 2010, 24(10): 5773–5780
32. Bhagiyalakshmi M, Lee J Y, Jang H T. Synthesis of mesoporous magnesium oxide: Its application to CO_2 chemisorption. International Journal of Greenhouse Gas Control, 2010, 4(1): 51–56
33. Bian S W, Baltrusaitis J, Galhotra P, Grassian V H. A template-free, thermal decomposition method to synthesize mesoporous MgO with a nanocrystalline framework and its application in carbon dioxide adsorption. Journal of Materials Chemistry, 2010, 20(39): 8705–8710
34. Jeon H, Min Y J, Ahn S H, Hong S-M, Shin J-S, Kim J H, Lee K B. Graft copolymer templated synthesis of mesoporous MgO/TiO_2 mixed oxide nanoparticles and their CO_2 adsorption capacities. Colloids and Surfaces a-Physicochemical and Engineering Aspects, 2012, 414: 75–81
35. She L, Li J, Wan Y, Yao X D, Tu B, Zhao D Y. Synthesis of ordered mesoporous MgO/carbon composites by a one-pot assembly of amphiphilic triblock copolymers. Journal of Materials Chemistry, 2011, 21(3): 795–800
36. Wang Q A, Luo J Z, Zhong Z Y, Borgna A. CO_2 capture by solid adsorbents and their applications: Current status and new trends. Energy & Environmental Science, 2011, 4(1): 42–55
37. Lee S C, Chae H J, Lee S J, Choi B Y, Yi C K, Lee J B, Ryu C K, Kim J C. Development of regenerable MgO-based sorbent promoted with K_2CO_3 for CO_2 capture at low temperatures. Environmental Science & Technology, 2008, 42(8): 2736–2741
38. Xiao G K, Singh R, Chaffee A, Webley P. Advanced adsorbents based on MgO and K_2CO_3 for capture of CO_2 at elevated temperatures. International Journal of Greenhouse Gas Control, 2011, 5(4): 634–639
39. Zhang K L, Li X H S, Duan Y H, King D L, Singh P, Li L Y. Roles of double salt formation and $NaNO_3$ in Na_2CO_3-promoted MgO absorbent for intermediate temperature CO_2 removal. International Journal of Greenhouse Gas Control, 2013, 12: 351–358
40. Lee S C, Choi B Y, Lee T J, Ryu C K, Soo Y S, Kim J C. CO_2 absorption and regeneration of alkali metal-based solid sorbents. Catalysis Today, 2006, 111(3-4): 385–390
41. Kim K, Han J W, Lee K S, Lee W B. Promoting alkali and alkaline-earth metals on MgO for enhancing CO_2 capture by first-principles calculations. Physical Chemistry Chemical Physics, 2014, 16(45): 24818–24823
42. Watanabe S, Ma X L, Song C S. Characterization of structural and surface properties of nanocrystalline TiO_2-CeO_2 mixed oxides by XRD, XPS, TPR, and TPD. Journal of Physical Chemistry C, 2009, 113(32): 14249–14257
43. Han K K, Zhou Y, Chun Y, Zhu J H. Efficient MgO-based mesoporous CO_2 trapper and its performance at high temperature. Journal of Hazardous Materials, 2012, 203: 341–347
44. Yong Z, Mata V, Rodriguez A E. Adsorption of carbon dioxide onto hydrotalcite-like compounds (HTlcs) at high temperatures. Industrial & Engineering Chemistry Research, 2001, 40(1): 204–209
45. Wang Q, Tay H H, Guo Z, Chen L, Liu Y, Chang J, Zhong Z, Luo J, Borgna A. Morphology and composition controllable synthesis of Mg-Al-CO_3 hydrotalcites by tuning the synthesis pH and the CO_2 capture capacity. Applied Clay Science, 2012, 55: 18–26
46. Li B, Wen X, Zhao N, Wang X Z, Wei W, Sun Y H, Ren Z H, Wang Z J. Preparation of high stability MgO-ZrO_2 solid base and its high temperature CO_2 capture properties. Journal of Fuel Chemistry and Technology, 2010, 38: 473–477
47. Kruk M, Jaroniec M. Gas adsorption characterization of ordered organic-inorganic nanocomposite materials. Chemistry of Materials, 2001, 13(10): 3169–3183
48. Klug H P, Alexander L E. X-ray Diffraction Procedures for Polycrystalline and Amorphous Materials. New York: Wiley, 1954
49. Zukal A, Kubů M, Pastva J. Two-dimensional zeolites: Adsorption of carbon dioxide on pristine materials and on materials modified by magnesium oxide. Journal of CO_2 Utilization, 2017, 21: 9–16
50. Pirngruber G D, Raybaud P, Belmabkhout Y, Cejka J, Zukal A. The role of the extra-framework cations in the adsorption of CO_2 on faujasite Y. Physical Chemistry Chemical Physics, 2010, 12(41): 13534–13546
51. Park D H, Lakhi K S, Ramadass K, Kim M K, Talapaneni S N, Joseph S, Ravon U, Al-Bahily K, Vinu A. Energy efficient synthesis of ordered mesoporous carbon nitrides with a high nitrogen content and enhanced CO_2 capture capacity. Chemistry (Weinheim an der Bergstrasse, Germany), 2017, 23(45): 10753–10757